ARTICLE

FT-IR, XPS, and DFT Study of Adsorption Mechanism of Sodium Acetohydroxamate onto Goethite or Hematite

Meng Wang[a], Hui-ping Hu[a*], Qi-yuan Chen[a], Guang-fu Ji[b]

a. College of Chemistry and Chemical Engineering, Central South University, Changsha 410083, China
b. Laboratory for Shock Wave and Detonation Physics Research, Institute of Fluid Physics, Chinese Academy of Engineering Physics, Mianyang 621900, China

(Dated: Received on August 27, 2015; Accepted on November 10, 2015)

The adsorption of sodium acetohydroxamate on the goethite or hematite surface was investigated by Fourier transform infrared spectroscopy (FT-IR), X-ray photoemission spectroscopy and periodic plane-wave density functional theory (DFT) calculations. The core-level shifts and charge transfers of the adsorbed surface iron sites calculated by DFT with periodic interfacial structures were confronted to the X-ray photoemission experiments. FT-IR results reveal that the interfacial structure of sodium acetohydroxamate adsorbed on the goethite or hematite surface may be assigned to a five-membered ring complex. In agreement with the adsorption energies determined by the DFT calculations, a five-membered ring complex is formed via bonding of one surface iron atom of goethite (101) or (100) to both oxygen atoms of hydroxamate group, and these two oxygen atoms of the hydroxamate group correspondingly attach to two neighboring iron atoms of the goethite surface. But a five-membered ring complex between two oxygen atoms of the hydroxamate group and one surface iron atom of hematite (001) is formed without any extra attachments. The calculated core-level shifts of Fe2p for the interfacial structures are correspondingly in good agreement with the experimental observed one, which confirmed the reliability of the calculated results.

Key words: Goethite, Hematite, Sodium acetohydroxamate, Adsorption, Fourier transform infrared spectroscopy, X-ray photoemission spectroscopy

I. INTRODUCTION

Hydroxamate derivatives, which are able to be adsorbed on metal (hydr)oxide surfaces, have long been sought due to its importance in flotation processes [1, 2]. Goethite and hematite are the dominant iron gangue minerals with high surface areas and high density of reactive surface sites [3]. The flotation of goethite and hematite can be directly undertaken using hydroxamate collectors. In a study of micro-flotation of goethite, Fuerstenau *et al.* found that full recovery of goethite was achieved from pH=5 to 10 at an octyl hydroxamate concentration of 0.3 mmol/L [2]. Fuerstenau *et al.* also suggested that a more satisfactory concentrate grade of hematite could be obtained with octyl hydroxamate than with oleate as collectors under the same flotation condition, and an optimum flotation was achieved in the vicinity of pH=8 to pH=9 [4]. However, hydroxamate collectors are now being employed increasingly in the flotation of copper oxide or rare earth ores, to achieve an acceptable grade of valued minerals when goethite and hematite are present as gangue minerals, and superior strategies to optimize the depression of goethite or hematite are required [1]. In order to facilitate the development of such strategies, it is advantageous to have a molecular-level understanding of the interfacial structure of hydroxamate derivatives on the goethite or hematite surface.

The interfacial structures of hydroxamate derivatives on iron (hydr)oxide surfaces were commonly investigated via Fourier transform infrared spectroscopy (FT-IR) [5, 6]. Although interfacial structures of hydroxamate derivatives on iron (hydr)oxide surfaces were all regarded as five-membered ring complexes, different or even conflicting FT-IR spectra of hydroxamate derivatives on iron (hydr)oxide surfaces were collected by different researchers [5, 6]. Holmen *et al.* proposed that a five-membered ring complex between surface iron atom of goethite and acetohydroxamic acid may be formed [5], because there exists a downshift of the C=O stretching vibration band and a upshift of the C−N stretching vibration band for adsorbed acetohydroxamic acid relative to the free acetohydroxamic acid. However, Borer *et al.* investigated the adsorption of desferrioxamine B to lepidocrocite (γ-FeOOH) via attenuated total reflectance (ATR) FT-IR, and found that the coordination of hydroxamate groups to surface iron atom of lepidocrocite resulted in

*Author to whom correspondence should be addressed. E-mail: phuhuiping@126.com, Tel.: +86-731-8877364

no shift of thehydroxamate C=O stretching vibration band (at 1578 cm^{-1}), but the N−OH bending vibration or C−N stretching vibration band at 1472 cm^{-1} downshifted to a rather intense band at 1463 cm^{-1} for the adsorbed desferrioxamine B [6]. Therefore, accurate interfacial structures of hydroxamate derivatives on iron (hydr)oxide surfaces could not be clearly identified just by FT-IR spectra.

X-ray photoelectron spectroscopy (XPS) is one of the most extensively used surface analytical techniques due to its high sensitivity of 0.1% [7] and the ability to probe the electronic and geometric structures of solid surface with adsorbed molecules [8]. In this technique, the binding energies of emitted core electrons are determined through their escape kinetic energy. When referred to a given reference, these binding energies can be expressed as core-level shifts which characterize the local atomic coordination and the relative oxidation state [9].

Density functional theory (DFT) calculations are suitable for a variety of surface science applications [10]. James *et al.* employed plane-wave DFT with an ultrasoft pseudopotential approximation and periodic geometries to study the adsorption of phosphate on the (100), (010), (001), (101), and (210) surfaces of goethite, and found that the (101) and (100) surfaces of goethite own higher reactivity [11]. Spin-polarized DFT calculations were carried out to model analogs of arsenic surface complexes on the hematite (001) surface [10]. Furthermore, the adsorption and reaction of SO_2 on clean and oxygen-precovered Pd (100) were investigated with XPS and DFT calculations, and the adsorbed SO_2 species were identified by comparing the calculated core level shifts (CLS) with experimental photoemission CLS [12]. This (incomplete, but demonstrative) summary represents the emerging role of, and growing interest in, DFT modeling applied to chemical questions about environmental interface reactivity.

In this work, sodium acetohydroxamate (aHA) was chosen as a model of hydroxamate collectors in the flotation of minerals. Goethite (101) surface, goethite (100) surface or hematite (001) surface, which represents the high reactivity properties of goethite or hematite, is taken into account. A combination of FT-IR, XPS, and DFT calculation is performed to study the interfacial structure of aHA bound to the goethite or hematite surface in the vicinity of pH=8 to pH=9. Modeling of the structures, energetics, electronic structures and core level shifts of aHA on goethite (100) and (101) or hematite (001) surface is performed in a self-consistent manner. Possible interfacial structures of aHA on (100) and (101) surfaces of goethite or (001) surface of hematite and the relative stabilities of the interfacial structures are obtained. And CLS of Fe2p and charge transfers of adsorbed surface iron site calculated by DFT with periodic interfacial structures are confronted to the X-ray photoemission experiments.

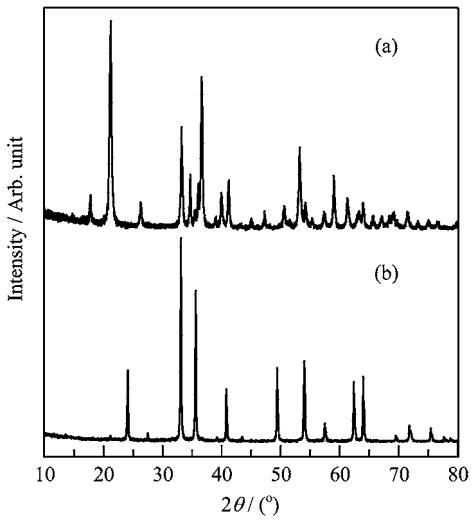

FIG. 1 XRD patterns of (a) goethite and (b) hematite.

II. METHODS

A. Experiments

Goethite and hematite were prepared according to the procedure of Schwertmann and Cornell [13], then dried at 60 °C for 24 h. The resulting particles of goethite or hematite were identified by X-ray powder diffraction pattern on X-ray diffractometer (D/max 2500, Rigaku Corporation, Cu Kα radiation, Japan). The XRD patterns are presented in Fig.1. The surface area and particle size distribution were measured by adsorption/desorption N_2(g) isotherm (Monosorb Autosorb, Quantachrome Instruments Ltd., USA) and laser diffraction (Mastersizer 2000, Malvern Instruments Ltd., UK), respectively. The results are given in Table I. aHA was of analytical grade.

The technique used for adsorbing aHA (Fig.2) on the goethite or hematite surface was modified from that developed by Jones *et al.*[14]. 0.25 g goethite or hematite was placed in an airtight conical flask with 50 mL of 0.001 mol/L sodium hydroxide solution and sonicated at 60 °C for 10 h to obtain a suspension, and the suspension was centrifuged for 30 min at 4000 r/min to separate the supernatant and the solid. The supernatant was decanted to obtain a fresh, carbonate-free goethite or hematite solid placed in an airtight conical flask. 50 mL aHA aqueous solution at pH=8.7 was added to the conical flask with 0.25 g of carbonate-free goethite or hematite solid, and the molar ratio for hydroxamate groups of aHA to ferric ion of goethite or hematite is 10:1. After the mixture was sonicated at 60 °C for 10 h and equilibrated for 24 h, the mixture was centrifuged at 4000 r/min to obtain a solid, and the solid was washed with de-ionized water for one time and dried in a vacuum oven at 60 °C for 24 h. The samples of goethite or hematite after the treat-

DOI:10.1063/1674-0068/29/cjcp1508182

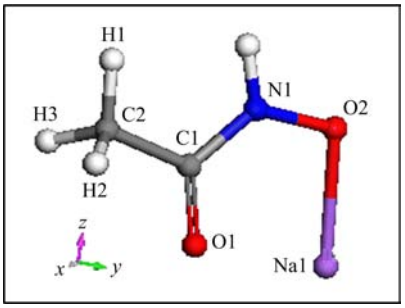

FIG. 2 The optimized structure of aHA.

TABLE I Properties of goethite and hematite samples.

Sample	Surface area	Particle size/μm			XRD
	/(m^2/g)	D10	D50	D90	JCPDS-PDF
Goethite	1.4	2.224	8.367	36.095	29-0713
Hematite	5.0	0.530	1.685	9.828	01-089-0596

ment of aHA (aHA-treated goethite or hematite) were obtained. Goethite or hematite before the treatment of aHA (untreated goethite or hematite) was prepared in the same manner except that aHA was not added to the carbonate-free goethite or hematite suspension.

The infrared spectra of the samples were measured by a Nicolet-6700 FT-IR spectrometer. The samples were analyzed on X-ray photoelectron spectrometer (ESCALAB 250XI, Thermo Scientific Co., USA) utilizing a monochromatic Al Kα X-ray at 1486.6 eV. All measurements were carried out at the pressure below 10^{-8} Pa and with a flood gun for charge neutralization. All spectra were charge-referenced so that the unfunctionalized aliphatic C1s component occurs at 284.8 eV. Curve fittings of Fe2p spectra were performed using the Avantage software, the reduced chi-squared (χ^2) value incorporated in the Avantage was used as a potentially useful guide to assess the fitting quality.

B. Calculation

Periodic slab models of the goethite surfaces were created by cleaving the respective surfaces (101) [15] and (100) [16] from the experimental crystal structure of bulk goethite (space group Pnma [17, 18]), which are modeled in a supercell geometry with a vacuum of 10 Å and extended to (1×3). The thickness of the slabs amounted to eight iron layers for goethite (101) and four for goethite (100), respectively. The periodic slab model of hematite surface was created by cleaving the surface (001) from the structure of bulk hematite (space group R$\bar{3}$c [19]). The surface (001) of hematite was extended to (1×2) and modeled using a periodic slab consisting of 6 O layers and 12 Fe layers on which the terminal Fe atoms contain triply-coordinated oxygen atoms in the subsurface layer, with an excess of 15 Å of vacuum separating the periodic images in the direction along the surface normal [10]. Initial magnetic moments of Fe atoms were assigned so as to obtain an antiferromagnetic goethite and hematite slab in each case. The goethite (101), (100) or hematite (001) surfaces was passivated by water dissociation products to surface dangling Fe and O atoms (as shown in Fig.3). The free aHA was added to goethite (101), (100) surfaces or hematite (001) surface in bidentate mononuclear structures (BM structures) as a model of aHA-goethite (101) system, aHA-goethite (100) system or aHA-hematite (001) system, respectively (as shown in Fig.4).

DFT calculations were carried out with the Castep Code [20, 21] in Materials Studio 6.0 using DFT. Plane wave basis sets were used to solve the Kohn-Sham equations. The GGA electron exchange and correlation effects were described using the Perdew Burke Ernzerhof (PBE) [22]. The on-site Coulomb interaction of 3d electrons, the GGA+U method was applied to the Fe atoms to improve the description of the electronic properties, the suggested values of the Hubbard U were correspondingly 5 eV for goethite [23] and 2.5 eV for hematite [24]. For the electronic integration in reciprocal space, the Brillouin zone was sampled according to the Monkhorst-Pack scheme [25]. A single k point was used for aHA, k points set was fine in calculation for surfaces with or without aHA.

For aHA, the ionic cores were described by the norm conserving pseudopotentials [26]. The wave functions were expanded with an energy cutoff of 750 eV for the geometry optimization and vibrational analysis. All positions were relaxed and fully optimized up to a force convergence of 0.03 eV/Å. The absence of imaginary frequencies verified that all structures were true minima [27]. The final structure of the geometry optimization was subjected to a single-point energy calculation with the ultrasoft pseudopotentials [28] and an energy cutoff of 340 eV for the plane-wave basis set to achieve an accuracy of total energy differences of 20 μeV/atom.

As to the models of surface slabs, aHA-goethite systems and aHA-hematite system, the geometry optimization was carried out with the same optimized level as the single-point energy calculation for aHA. The structures of the adsorbate and the four outer iron layers of goethite (101) surface, the adsorbate and the two outer iron layers of goethite (100) surface or the adsorbate and the two outer iron layers of hematite (001) surface were relaxed and fully optimized up to a force convergence of 0.05 eV/Å, while the inner layers kept fixed at their bulk positions to reproduce the properties of bulk goethite or hematite.

The adsorption energy, $E_{\rm ads}$, of the adsorbate at goethite or hematite surface was described as:

$$E_{\rm ads} = E_{\rm adsorbate\text{-}surface} - E_{\rm surface} - E_{\rm adsorbate} \quad (1)$$

where $E_{\rm surface}$ and $E_{\rm adsorbate\text{-}surface}$ are the total energy of goethite or hematite surface slabs before and after

DOI:10.1063/1674-0068/29/cjcp1508182

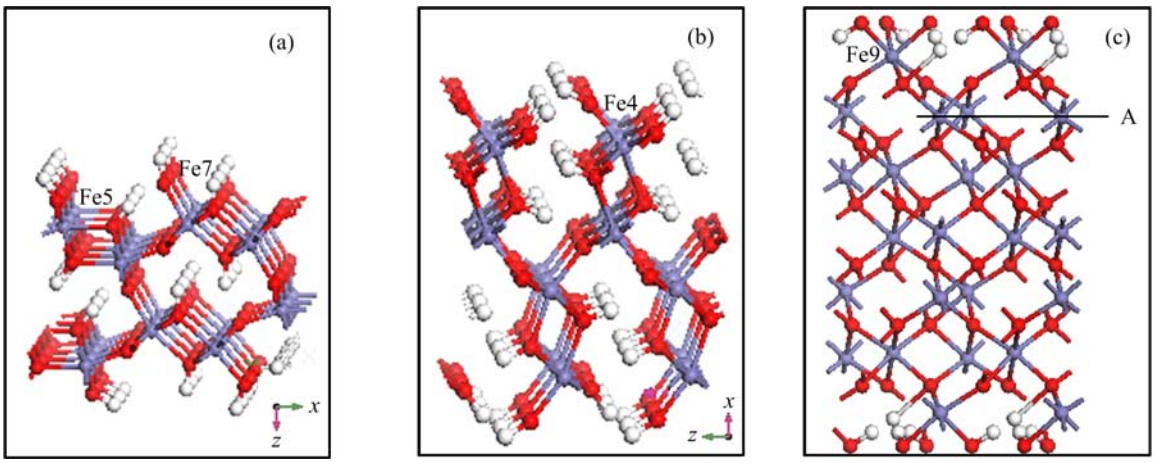

FIG. 3 Truncated side view of the model for (a) goethite (101), (b) goethite (100) and (c) hematite (001) surfaces. A horizontal line indicates a type-A termination is obtained by removing the atoms above the line. Oxygen atoms are shown in red, iron atoms in grayish blue and hydrogen atoms in white.

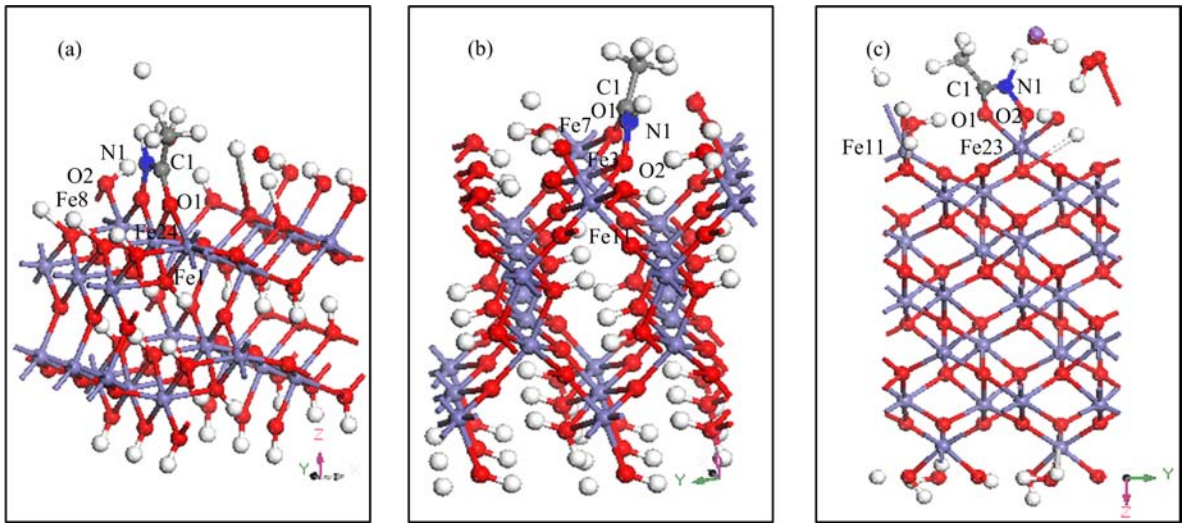

FIG. 4 Illustration of the optimized interfacial structures of aHA adsorbed on (a) goethite (101), (b) goethite (100), and (c) hematite (001) surface. Iron atoms are shown in purple, oxygen atoms in medium red, nitrogen atoms in blue and hydrogen atoms in white.

the adsorption of the adsorbate. $E_{\mathrm{adsorbate}}$ is the total energy of an isolated adsorbate molecule.

For the calculation of CLS of Fe2p, geometry-optimized aHA-goethite systems or aHA-hematite systems were used as models of interfacial structures. We modeled CLS of Fe2p as total energy differences between the system with a core hole on the excited Fe atom and the unperturbed system. To describe the excited Fe atom, we generated a special Fe pseudopotential on the basis of an electronic configuration of the atom which included a core hole in the 2p level. In a pseudopotential formulation, absolute binding energies were not accessible. However, CLS could be accurately achieved with respect to a given reference. In this work, the reference was taken to be the surface iron atoms located at the same position on goethite (101), (100) surfaces or hematite (001) surface. Within these calculations, we obtain Eq.(2) for the CLS of a single atom from the interfacial structures:

$$E_{\mathrm{CLS}} = (E_{\mathrm{ion}} - E_{\mathrm{gs}}) - (E_{\mathrm{ion}}^{\mathrm{ref}} - E_{\mathrm{gs}}^{\mathrm{ref}}) \qquad (2)$$

here, E_{CLS} is the core level shift of a certain system. E_{ion} and E_{gs} represent the ground state energies of system with and without a core hole, respectively.

III. RESULTS AND DISCUSSION

A. FT-IR spectroscopy analysis

The FT-IR spectra of aHA, untreated goethite, and aHA-treated goethite are depicted in Fig.5. The FT-IR

DOI:10.1063/1674-0068/29/cjcp1508182

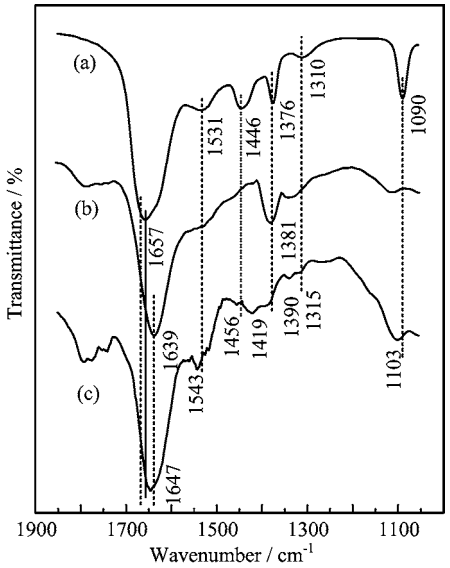

FIG. 5 FT-IR spectra of (a) aHA, (b) goethite, and (c) aHA-treated goethite.

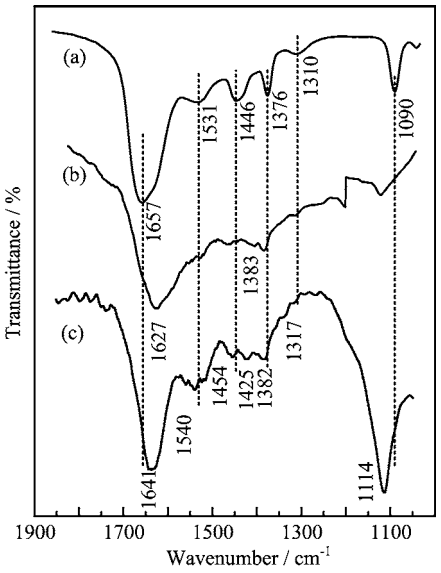

FIG. 6 FT-IR spectra of (a) aHA, (b) hematite, and (c) aHA-treated hematite.

spectra of aHA, untreated hematite, and aHA-treated hematite are depicted in Fig.6.

The vibrational spectrum of aHA exhibits characteristic vibrational modes in the wavenumber range of 1000−1800 cm^{-1} (Fig.5(a)). The band corresponding to C=O stretching vibration in aHA is located at 1657 cm^{-1} [29]. The weak broad band at 1531 cm^{-1} is a result of the coupling of weak N−H bending vibration band and C−N stretching vibration band. This broadening may be due to either coupling or overlapping with the NOH bending vibration. The band at 1446 and 1376 cm^{-1} are assigned to the CH_3 bending vibration [30], the C−N stretching vibration band is occurred at 1310 cm^{-1}, and the band at 1090 cm^{-1} is ascribed to the N−O stretching vibration [31].

As shown in Fig.5(b), the band at 1639 and 1381 cm^{-1} are assigned to OH bending vibration band of adsorbed water and constitutional water of the untreated goethite. As shown in Fig.6(b), the bands at 1627 and 1384 cm^{-1} are assigned to the vibration of adsorbed water and constitutional water of the untreated hematite.

In the FT-IR spectra of aHA-treated goethite (Fig.5(c)), the C=O stretching vibration band in aHA is downshifted from 1657 cm^{-1} to 1647 cm^{-1}, and the N−O stretching vibration band shifts to a higher wavenumber from 1090 cm^{-1} to 1103 cm^{-1}, the C−N stretching vibration bands which appear at 1531 and 1310 cm^{-1} considerably shift to a higher wavenumber (1543 and 1315 cm^{-1}) from their position in the unadsorbed aHA. In the FT-IR spectra of aHA-treated hematite (Fig.6(c)), the C=O stretching vibration band in aHA is downshifted from 1657 cm^{-1} to 1641 cm^{-1}, and the N−O stretching vibration band shifts to a higher wavenumber from 1090 cm^{-1} to 1114 cm^{-1}, the C−N stretching vibration bands which appear at 1531 and 1310 cm^{-1} considerably shift to a higher wavenumber (1540 and 1317 cm^{-1}) from their position in the unadsorbed aHA. These shifts in frequency indicate that the formation of five-membered ring weakens the carbonyl bond while increasing the N−O bond strength of the adsorbed aHA relative to that of unadsorbed aHA. Considering resonance within the five-membered ring, the C−N bond may also have more partial double-bond character in the adsorbed aHA. The results suggest that aHA is chemisorbed on the goethite or hematite surface and a five-membered ring may be formed through loss of the oxygen proton and binding of the surface iron of goethite or hematite to both oxygen atoms of aHA, which is also supported by the spectral resemblance to be previously published spectrum of Fe-acetohydroxamic acid complexes on the goethite surface [5].

B. XPS analysis

For the analysis of Fe2p spectra, a Shirley background is used for the $Fe2p_{1/2}$ and $Fe2p_{3/2}$ envelopes. The $Fe2p_{1/2}$ and $Fe2p_{3/2}$ envelopes are fitted using peaks corresponding to the Gupta and Sen (GS) multiplets, surface structures and shake-up satellites [32]. The main peak of GS-predicted multiplets for the $Fe2p_{3/2}$ envelope had a full width at half-maximum (FWHM) ranging from 1.0 eV to 1.4 eV and the relative intensities followed the GS predictions well. The peak ascribed to surface structures is added with a higher binding energy and a larger FWHM than the GS multiplets. A single large peak representing the satellites due to shake-up is also added. A single low intensity peak on

DOI:10.1063/1674-0068/29/cjcp1508182

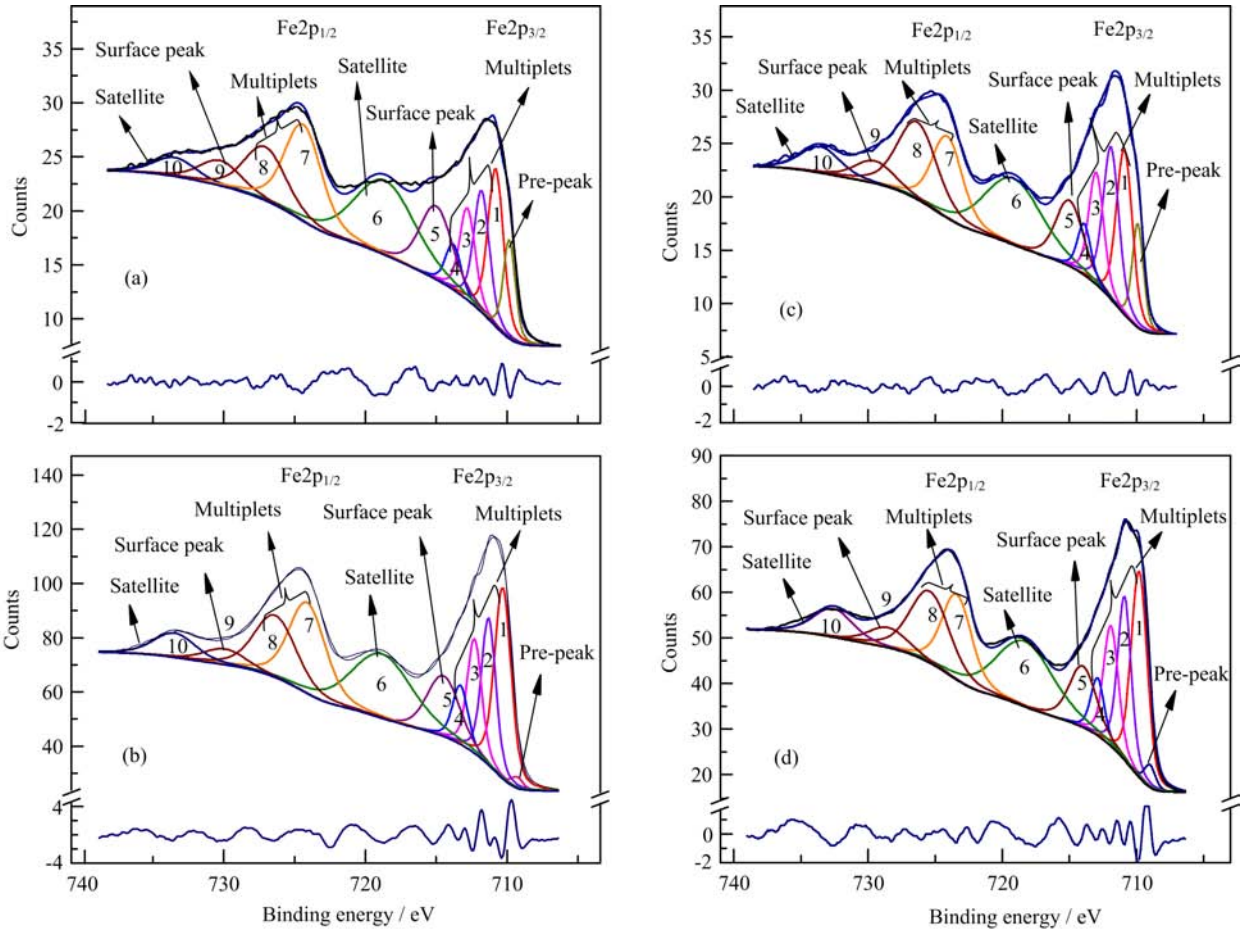

FIG. 7 The Fe2p spectra and the fitting curves of (a) goethite, (b) hematite, (c) aHA-treated goethite, and (d) aHA-treated hematite.

TABLE II The fitting peaks of Fe2p spectra for goethite or hematite before and after the treatment of aHA.

	Fitting peaks	Peak	Untreated goethite		aHA-treated goethite		Untreated hematite		aHA-treated hematite	
			Peak/eV	FWHM/eV	Peak/eV	FWHM/eV	Peak/eV	FWHM/eV	Peak/eV	FWHM/eV
$Fe2p_{3/2}$	Pre-peak		709.8	1.0	709.3	1.0	709.9	1.0	709.0	1.0
	Multiplets	1	710.8	1.3	710.3	1.4	710.9	1.4	709.8	1.4
		2	711.8	1.3	711.3	1.2	711.9	1.4	710.9	1.4
		3	712.8	1.3	712.3	1.2	713.0	1.3	711.9	1.3
		4	713.8	1.3	713.3	1.3	713.9	1.2	712.9	1.2
	Surface peak	5	715.0	2.7	714.5	2.7	715.0	2.4	714.0	2.4
	Satellite	6	718.5	5.0	718.8	5.0	719.2	5.0	718.3	5.0
$Fe2p_{1/2}$	Multiplets	7	724.4	3.1	724.1	3.1	724.1	2.7	723.4	2.7
		8	727.0	3.5	726.5	3.5	726.4	3.5	725.4	3.5
	Surface peak	9	730.3	3.5	729.9	3.5	729.5	3.5	728.5	3.5
	Satellite	10	733.5	3.5	733.5	3.5	733.6	3.5	732.6	3.5

the low-binding-energy side of the envelope is added to account for the information of Fe ions with a lower than normal oxidation state by the production of defects in neighboring sites, and this peak is referred to as the "pre-peak". After the Fe2p spectrum was fitted, the main peak centre of gravity (CG) was determined using the GS multiplets only, which is the peak 2 in the fitting curve. The Fe2p spectra and fitting curves for goethite or hematite before and after treatment of aHA are depicted in Fig.7. Table II lists the fitting peaks of the Fe2p envelopes for goethite or hematite before and after the treatment of aHA.

DOI:10.1063/1674-0068/29/cjcp1508182

TABLE III The interatomic distances Fe−O and the lattice parameters for optimized bulk goethite or hematite.

Items	Interatomic distances/Å		Lattice parameter	
	This work	Reference	This work	Reference
Bulk goethite	1.864	1.901 [37]	a=4.395 Å	a=4.598 Å [37]
	1.879 (×2)	1.979 (×2) [37]	b=9.510 Å	b=9.951 Å [37]
	1.993 (×2)	2.121 (×2) [37]	c=2.925 Å	c=3.018 Å [37]
	2.008	2.136 [37]	α=β=γ=90°	α=β=γ=90° [37]
Bulk hematite	2.000 (×3)	1.951 (×3) [38]	a=b=5.035 Å	a=b=5.037 Å [38]
	2.024 (×3)	2.103 (×3) [38]	c=13.720 Å	c=13.771 Å [38]
			α=β=90°, γ=120°	α=β=90°, γ=120° [38]

Values in parentheses give the number of bond.

As presented in Fig.7 and Table II, it is observed that the binding energies of all fitting peaks of Fe2p for goethite or hematite before the treatment of aHA were decreased compared with that after the treatment of aHA. Compared with CG and surface peaks at 711.8 and 715.0 eV in the $Fe2p_{3/2}$ envelope for untreated goethite, the CG and surface peaks in the $Fe2p_{3/2}$ envelope for aHA-treated goethite are correspondingly downshifted to 711.3 and 714.5 eV. As the same as the downshift observed on CG and surface peaks in the $Fe2p_{3/2}$ envelope for aHA-treated goethite, the peaks in Fe2p spectrum for aHA-treated goethite are correspondingly downshifted by 0.5 eV relative to untreated goethite. The binding energies of the CG and surface peaks in the $Fe2p_{3/2}$ envelope for untreated hematite are correspondingly 711.9 and 715.0 eV. The CG and surface peaks in the $Fe2p_{3/2}$ envelope for aHA-treated hematite are correspondingly downshifted to 710.9 and 714.0 eV. Compared with untreated hematite, the peaks in the Fe2p spectrum for aHA-treated hematite are both downshifted by 1.0 eV, which is the same as the downshift observed on the CG and surface peaks in the $Fe2p_{3/2}$ envelope for aHA-treated hematite.

In this work, the downshift of binding energies of Fe2p spectra for aHA-treated goethite or hematite will be explained by the atomic potential model [33]. The atomic potential model assumes that the atomic core potential varies linearly with the electron density of atoms, and the oxidation of one atom results in the increase of the atomic binding energy of the inner electron, whereas the reduction of one atom results in the decrease of the atomic binding energy of the inner electron. After aHA was adsorbed on the goethite or hematite surfaces, the binding energies of Fe2p spectra were correspondingly decreased with respect to untreated goethite or hematite. According to the atomic potential model, the iron atoms may be partially reduced to a lower valence state. The coordination between oxygen atoms of hydroxamate group from aHA and surface iron atoms of goethite or hematite may explain the partial reduction of iron atoms on the surfaces because these iron atoms accepted electron clouds from oxygen atoms of hydroxamate group from aHA. However, the binding energy shift of the peaks of Fe2p spectra for aHA-treated hematite was almost twice as much as that of aHA-treated goethite, which may be due to the differences of the interfacial structures between aHA-treated goethite and aHA-treated hematite.

C. Quantum chemical calculations

We present the optimized interfacial structure, energetics, electronic structures, and CLS of Fe2p of the five-memerbed ring of hydroxamate group adsorbed on goethite or hematite surfaces after a quantum chemical calculation of aHA adsorbed on the periodic surface slab of goethite or hematite was carried out.

1. Interfacial structures

The O^H-O^H distance (2.925 Å) at Fe site of goethite (101) or at Fe site of goethite (100) matches well with the O−O distance (2.817 Å) of aHA, which allows aHA to form a bidentate mononuclear (BM) structure on the goethite (101) and (100) surfaces. On the hematite (001) surface, the Fe−Fe distance is 5.035 Å, the O^H-O^H distance at one surface dangling iron atom of the hematite (001) surface passivated by the dissociative water functional groups is 2.622 Å, which also matches well with the O−O distance (2.817 Å) of aHA and thus also allows aHA to form a bidentate mononuclear (BM) structure. Here bidentate mononuclear (BM) structure, which specifies the linkage between aHA and surface iron site via two oxygen atoms of aHA as an idealized starting interfacial structure, was verified in detail (Fig.4).

The interatomic distances and lattice parameters for optimized bulk goethite or hematite are listed in Table III. The Fe−O distances in optimized bulk goethite are in the range from 1.864 Å to 2.008 Å, which owns a difference within 0.128 Å relative to the previously calculated data in the range from 1.901 Å to 2.136 Å for bulk goethite [34]. The Fe−O distances in optimized

DOI:10.1063/1674-0068/29/cjcp1508182

TABLE IV The calculated interatomic distances d (Å) and bond angles (°) for the aHA, interfacial structures of aHA adsorbed on goethite (101), (100) or hematite (001) surfaces.

	aHA-goethite (101)		aHA-goethite (100)		aHA-hematite (001)		Free aHA	
d_{Fe-O}	Fe24−O2	1.887	Fe3−O2	1.928	Fe23−O2	1.928		
	Fe24−O1	1.941	Fe3−O1	1.959	Fe23-O1	2.014		
	Fe8−O2	2.076	Fe11−O2	2.135				
	Fe16−O1	2.111	Fe7−O1	2.181	Fe11−O1	3.757		
d_{N-O}	N1−O2	1.380	N1−O2	1.379	N1−O2	1.390	N1−O2	1.355
d_{N-C}	N1−C1	1.353	N1−C1	1.340	N1−C1	1.319	N1−C1	1.349
d_{C-O}	C1−O1	1.288	C1−O1	1.295	C1−O1	1.314	C1−O1	1.271
∠O−Fe−O	O1−Fe24−O2	85.7	O1−Fe3−O2	82.9	O1−Fe23−O2	80.5		
∠Fe−O−C	Fe24−O1−C1	110.2	Fe3−O1−C1	106.4	Fe23−O1−C1	110.2		
∠Fe−O−N	Fe24−O2−N1	107.7	Fe3−O2−N1	102.2	Fe23−O2−N1	115.0		
∠O−C−N	O1−C1−N1	117.3	O1−C1−N1	116.9	O1−C1−N1	121.8	O1−C1−N1	122.6
∠C−N−O	C1−N1−O2	117.8	C1−N1−O2	117.6	C1−N1−O2	112.4	C1−N1−O2	125.0

bulk hematite are 2.000 and 2.024 Å, which is in agreement with the observed data of 1.9511 and 2.1028 Å from the single crystal of hematite [35]. The results illustrate the validity of the calculated method.

The interatomic distances and bond angles for the BM structures of aHA on goethite (101), (100) and hematite (001) surfaces are listed in Table IV. As listed in Table IV, after the goemetry optimization of the interfacial structures of aHA adsorbed on the goethite (101), (100) or hematite (001) surface, the average Fe−O distance for the BM structures is approximately 2 Å. Besides, the interatomic distances of Fe8−O2 and Fe16−O1 are correspondingly 2.076 and 2.111 Å in the interfacial structures of aHA adsorbed on goethite (101) surface, and the interatomic distances of Fe11−O2 and Fe7−O1 are correspondingly 2.135 and 2.181 Å in the interfacial structures of aHA adsorbed on goethite (100) surface. It can be observed that the interatomic distance between the neighboring iron atom and the oxygen atom of aHA almost equals to the average Fe−O distance of about 2 Å in the BM structures of aHA adsorbed on goethite (100) or (101) surface. Thus, the adsorbed aHA on goethite (101) and (100) forms a five-membered ring complex as a BM structure, and two oxygen atoms of aHA simultaneously attach to two neighboring surface iron atoms (Fig.4 (a) and (b)). Whereas, the interatomic distance of Fe11−O1 in the interfacial structures of aHA adsorbed on hematite (001) surface is 3.757 Å, which is much larger than the average Fe−O distance of about 2 Å in the BM structures. Therefore, the formation of a five-membered ring complex as a BM structure occurs on hematite (001) surface without any extra attachments between two oxygen atoms of aHA and the neighboring surface iron atoms (Fig.4(c)). This conclusion is in accordance with our assumption from FT-IR results (Fig.5 and Fig.6).

According to Ref.[36], the experimental geometric parameters of $[Fe(aha)_3]$ (aha^-=acetohydroxamate anion)

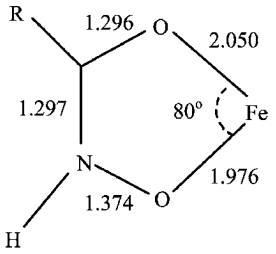

FIG. 8 Model compounds of $[Fe(aha)_3]$ (aha^- is acetohydroxamate) labeled with key interatomic distances in Å and the bond angel [36].

obtained by Fe L-edge X-ray absorption spectroscopy are given in Fig.8. The calculated geometric parameters of the optimized interfacial structure of aHA-hematite (001) almost equal to that shown in Fig.8, which means that the optimized interfacial structure of aHA-hematite (001) is reasonable. The calculated geometric parameters of the optimized interfacial structure of aHA-goethtie (100) are much closer to that shown in Fig.8 than the calculated geometric parameters of the optimized interfacial structure of aHA-goethtie (101). This indicates that the optimized interfacial structure of aHA-goethtie (100) is more reasonable.

2. Adsorption energies of the optimized interfacial structures

The calculated adsorption energies of aHA adsorbed on goethite (101), (100), and hematite (001) surfaces are −1.59, −2.65, and −6.76 eV. On the basis of these results, goethite (101), (100) or hematite (001) surfaces are predicted to be capable of adsorbing aHA. The most energetically favorable interfacial structure is the BM complex of aHA adsorbed on hematite (001) with E_{ads} of −6.76 eV. The adsorption energies of the BM complex of aHA adsorbed on goethite (101) and (100) sur-

DOI:10.1063/1674-0068/29/cjcp1508182

TABLE V Calculated Mulliken charges, charge transfer, and calculated CLS of atoms.

Structure	Atom	Mulliken charge of atoms/e	Charge transfer/e	CLS/eV
aHA	N1	−0.34		
	O1	−0.72		
	O2	−0.71		
Goethite (101)	Fe5	1.01		
Goethite (100)	Fe4	1.08		
Hematite (001)	Fe9	1.17		
aHA adsorbed on goethite (101)	N1	−0.40		
	O1	−0.50		
	O2	−0.55		
	Fe8	0.99	−0.02	−0.44
	Fe16	1.00	−0.01	−0.46
	Fe24	1.04	+0.03	−0.27
aHA adsorbed on goethite (100)	N1	−0.28		
	O1	−0.51		
	O2	−0.43		
	Fe3	1.07	−0.01	−0.57
	Fe7	1.07	−0.01	−0.59
	Fe11	1.05	−0.03	−0.62
aHA adsorbed on hematite (001)	N1	−0.31		
	O1	−0.55		
	O2	−0.45		
	Fe11	1.10	−0.07	−1.05
	Fe23	1.05	−0.12	−1.08

face are correspondingly −1.59 and −2.65 eV.

3. Electronic properties and core level shifts

The electronic structures and core level shifts of the interfacial structures of aHA adsorbed on goethite (101), (100), or hematite (001) surfaces were calculated. The calculated Mulliken charges, charge transfer and CLS values of atoms are listed in Table V.

As shown in Table V, the negative charges of aHA are mainly clustered on O1, N1, and O2 atoms of hydroxamate group. Hence O1 and O2 atoms in hydroxamate group of aHA are the electron-donating centers and the chemically reactive centers. After the adsorption of aHA on the goethite (101), (100), or hematite (001) surfaces occurred, the charges of two oxygen atoms of the hydroxamate group increased, and the charges of the adsorbed surface Fe sites decreased. This means that electron clouds are transferred from O atoms of hydroxamate group to adsorbed surface Fe sites on the goethite (101), (100), or hematite (001) surfaces, and the transferred electrons are mainly localized at the adsorbed surface Fe atoms or their nearest neighboring iron atoms. Therefore, the Fe2p surface peaks of the adsorbed surface iron sites may appear at lower binding energy than that of unadsorbed surface iron atoms at clean mineral surfaces. As described in Refs.[37, 38], the CLS is roughly proportional to the charge transfer. Here we compare the calculated charge transfers and CLS with the experimental Fe2p core level photoemission measurements. We consider that the consistence between the calculated CLS and the experimental observed CLS is a good indicator of the pertinence of our model.

According to experimental results (Table II), the surface peaks for aHA-treated goethite are downshifted by 0.5 eV compared with untreated goethite. According to the calculated results (listed in Table V), the calculated charge transfer for adsorbed Fe2 sites on goethite (101) surface is 0.02 e, and the calculated CLS of Fe2p (−0.44 eV) is consistent with the experimentally observed Fe2p CLS of Fe2p (−0.5 eV). The calculated charge transfer of adsorbed surface Fe3 sites on goethite (100) surface is −0.01 e, and the calculated CLS of Fe2p (−0.57 eV) is in good agreement with the experimentally observed CLS of Fe2p (−0.5 eV). Thus, the goethite (101) and (100) surfaces may be predicted to be capable of adsorbing aHA as a BM structure. On the other hand, the surface peaks for aHA-treated hematite are downshifted by 1.0 eV relative to untreated hematite on the basis of the experimental data (Table II). Our calculated charge transfer of adsorbed surface iron sites on hematite (001) surface

DOI:10.1063/1674-0068/29/cjcp1508182

is 0.12 e, and the calculated CLS of Fe2p (−1.08 eV) is in good agreement with the experimentally observed CLS of Fe2p (−1.0 eV). This consistency between the calculated CLS and the experimentally observed CLS of Fe2p suggests that our optimized interfacial structure for aHA-hematite (001) system can be regarded as a reasonable and realistic structure. Furthermore, due to the extra bond to the neighboring iron atoms in the aHA-goethite system, the calculated or the observed CLS of the surface peaks of Fe2p spectra for aHA-treated hematite was almost twice as much as that of aHA-treated goethite. With the combination of the calculated adsorption energies (Table V), we can conclude that the goethite (101), (100), and hematite (001) surfaces are the favorable surfaces for aHA adsorption.

IV. CONCLUSION

The adsorption of aHA on goethite or hematite surface was investigated by FT-IR, XPS and DFT calculations, respectively. All the results reveal that the interfacial structures of aHA adsorbed on the goethite or hematite surface are assigned to five-membered ring complexes.

The goemetry optimization by DFT indicates that the adsorbed aHA on goethite (101) and (100) forms a five-membered ring complex as a BM structure, and two oxygen atoms of aHA simultaneously attach to two neighboring surface iron atoms. Whereas, the formation of a five-membered ring complex as a BM structure occurs on hematite (001) surface without any extra attachments between two oxygen atoms of aHA and the neighboring surface iron atoms.

The calculated CLS (−0.44 eV) of Fe2p for the interfacial structure on goethite (101) surface was consistent with the experimental observed CLS of Fe2p (−0.5 eV), and the calculated CLS of Fe2p (−0.57 eV) for the interfacial structure on goethite (100) surface is in good agreement with the experimentally observed CLS of Fe2p (−0.5 eV). Thus, the goethite (100) and (101) surfaces may be predicted to be capable of adsorbing aHA as a BM structure. On the other hand, for the interfacial structure on hematite (001) surface, the calculated CLS of Fe2p (−1.08 eV) is in good agreement with the experimentally observed CLS (−1.0 eV). This consistency between the calculated CLS and the experimentally observed CLS of Fe2p confirms the reasonability of the optimized interfacial structure for aHA-hematite (001) system.

V. ACKNOWLEDGMENTS

This work was supported by the National Natural Science Foundation of China (No.51134007 and No.51174231).

[1] A. N. Buckley and G. K. Parker, Inter. J. Mineral Proces. **121**, (2013).
[2] M. C. Fuerstenau, J. D. Miller, and G. Gutierrez, AIME Trans. **238**, (1967).
[3] U. Schwertmann and R. M. Cornell, *The Iron Oxides-Structure, Properties, Reactions, Occurrences and Uses*, Wiley-VCH, (2003).
[4] M. C. Fuerstenau, R. W. Harper, and J. D. Miller, AIME Trans. **247**, (1970).
[5] B. A. Holmén, M. I. Tejedor-Tejedor, and W. H. Casey, Langmuir **13**, 8 (1997).
[6] P. Borer, S. J. Hug, B. Sulzberger, S. M. Kraemer, and R. Kretzschmar, Geochimica et Cosmochimica Acta **73**, 16 (2009).
[7] C. Zhao, *Ph. D. Dissertation*, Blacksburg, Virginia: Virginia Polytechnic Institute and State University, (2014).
[8] Z. Zeng, X. Ma, W. Ding, and W. Li, Sci. China Chem. **53**, 2 (2010).
[9] G. Miceli and A. Pasquarello, Appl. Phys. Lett. **102**, 20 (2013).
[10] C. J. Goffinet and S. E. Mason, J. Environmental Monitoring: JEM **14**, 7 (2012).
[11] J. D. Kubicki, K. W. Paul, L. Kabalan, Q. Zhu, M. K. Mrozik, M. Aryanpour, A. M. Pierre-Louis, and D. R. Strongin, Langmuir **28**, 41 (2012).
[12] N. Luckas, K. Gotterbarm, R. Streber, M. P. A. Lorenz, O. Hoefert, F. Vines, C. Papp, A. Goerling, and H. P. Steinrueck, Phys. Chem. Chem. Phys. **13**, 36 (2011).
[13] U. Schwertmann and R. M. Cornell, *Iron Oxides in the Laboratory: Preparation and Characterization*, New York: Wiley-VCH, (1991).
[14] F. Jones, J. B. Farrow, and W. van Bronswijk, Langmuir **14**, 22 (1998).
[15] M. Villalobos, M. A. Cheney, and J. Alcaraz-Cienfuegos, J. Colloid interface Sci. **336**, 2 (2009).
[16] R. M. Cornell, A. M. Posner, and J. P. Quirk, J. Inorg. Nuclear Chem. **36**, 9 (1974).
[17] A. Manceau, K. L. Nagy, L. Spadini, and K. V. Ragnarsdottir, J. Colloid Interface Sci. **228**, 2 (2000).
[18] K. W. Paul, J. D. Kubicki, and D. L. Sparks, Eur. J. Soil Sci. **58**, 4 (2007).
[19] A. Rohrbach, J. Hafner, and G. Kresse, Phys. Rev. B **70**, 12 (2004).
[20] Y. Li, Y. Gao, B. Xiao, T. Min, Z. Fan, S. Ma, and L. Xu, J. Alloys Compd. **502**, 1 (2010).
[21] K. Refson, P. R. Tulip, and S. J. Clark, Phys. Rev. B **73**, 15 (2006).
[22] J. P. Perdew, K. Burke, and M. Ernzerhof, Phys. Rev. Lett. **77**, 18 (1996).
[23] K. Otte, W. W. Schmahl, and R. Pentcheva, J. Phys. Chem. C, **117**, 30 (2013).
[24] H. Guo and A. S. Barnard, Phys. Rev. B **83**, 094112 (2011).
[25] H. J. Monkhorst and J. D. Pack, Phys. Rev. B **13**, 12 (1976).
[26] D. R. Hamann, M. Schlüter, and C. Chiang, Phys. Rev. Lett. **43**, 20 (1979).
[27] H. Tavakol, J. Mol. Struct.: THEOCHEM **916**, 1 (2009).

DOI:10.1063/1674-0068/29/cjcp1508182

[28] K. Laasonen, R. Car, C. Lee, and D. Vanderbilt, Phys. Rev. B **43**, 8 (1991).
[29] H. S. Alkhatib, M. O. Taha, and K. M. Aiedeh, Eur. Polymer J. **42**, 10 (2006).
[30] D. C. Edwards, S. B. Nielsen, A. A. Jarzęcki, T. G. Spiro, and S. C. B. Myneni, Geochimica et Cosmochimica Acta **69**, 13 (2005).
[31] Angela G. Stewart, Karen A. Hudson-Edwards, and William E. Dubbin, Geochimica et Cosmochimica Acta **115**, 1 (2013).
[32] A. P. Grosvenor, B. A. Kobe, M. C. Biesinger, and N. S. McIntyre, Surf. Interface Anal. **36**, 12 (2004).
[33] R. J. Cole, D. A. C. Gregory, and P. Weightman, Phys. Rev. B **49**, 8 (1994).
[34] M. Blanchard, E. Balan, P. Giura, K. Béneut, H. Yi, G. Morin, C. Pinilla, M. Lazzeri, and A. Floris, Phys. Chem. Minerals **41**, 4 (2013).
[35] V. A. Sadykov, L. A. Isupova, S. V. Tsybulya, S. V. Cherepanova, G. S. Litvak, E. B. Burgina, G. N. Kustova, V. N. Kolomiichuk, V. P. Ivanov, E. A. Paukshtis, A. V. Golovin, and E. G. Avvakumov, J. Solid State Chem. **123**, (1996).
[36] Rosalie K. Hocking, Serena DeBeer George, Kenneth N. Raymond, Keith O. Hodgson, Britt Hedman, and A. E. I. Solomon, J. Am. Chem. Soc. **132**, 4006 (2010).
[37] J. Wang and I. Lefebvre, J. Phys. Chem. C **115**, 46 (2011).
[38] Z. Q. Jiang, W. H. Zhang, L. Jin, X. Yang, F. Q. Xu, J. F. Zhu, and W. Huang, J. Phys. Chem. C **111**, 12434 (2007).

DOI:10.1063/1674-0068/29/cjcp1508182